INTERNATIONAL JOURNAL OF INTELLIGENT CONTROL AND SYSTEMS
VOL. 12, NO. 3, SEPTEMBER 2007, 254-263

Design and Modeling of an Interactive Mobile Aqua Probe and Surveillance (IMAPS) System

Hong ZHANG and Ying TANG

***Abstract*— In this paper, we introduce the development of the Interactive Mobile Aqua Probe and Surveillance (IMAPS) system. It is a new version of autonomous surface craft that can communicate with users in real time and reach underwater using its onboard winch and sensor system. A graphical user interface is designed and an initial modeling of the robot is performed to provide a stepping stone for future autonomous control. Experimental result shows that the system is highly efficient and is ready to perform many demanding tasks in various water and weather conditions.**

***Index Terms* – Mobile Robot, Agent-Server, Surface Vehicle**

1. INTRODUCTION

Ecological and biological studies of aquatic habitats, especially those in shallow-water, are often hindered by difficulties of accessing remote sites or the cost of collecting high resolution data in space and time. For example, physical sampling at predetermined locations by workers in the field [15] offers limited sampling stations and numbers of observations (discrete in time, continuous in space). Such methods are sensitive to environmental and logistical conditions (e.g. season, weather, terrain, access), which could influence the choice of sampling times and sites. In contrast, mounting fixed sensors in the field (e.g., distributed sensors [4, 12] or buoy stations [11]) allows continuous monitoring of a specific and static location (continuous in time, discrete in space). However, the deployment of mounted sensors in the field can physically alter the environment by their presence and the cost of this option multiplies quickly with the number of stations. Moreover, both of these sampling regimes lack the flexibility that is critical to characterizing conditions or organisms in dynamic habitats. With the technology advances, satellite or airborne sensors [20] offer an alternative method for a semi-continuous ultra-wide range monitoring of a targeted area. Due to the nature of radio-frequency, this method is highly restricted by water depth and is technically difficult or expensive to focus on an area of interest for a long period of time.

On the other hand, mobile sensor platforms such as Remotely Operated Vehicles (ROV) [20, 23] and Autonomous Underwater Vehicles (AUV) [6, 13] are capable of dynamic remote data collection. However, these vehicles are often designed for use in the deep environments of the open ocean. Their cost, size, and limited agility are not suitable for work in other aquatic habitats (e.g., shallow water).

Recently, there is some limited development of Autonomous Surface Crafts (ASC) [1, 8]. However, they are mostly based on sea-going vehicles such as kayaks [7] or sail boats [14]. Hence, they suffer from the same limitations as ROV and AUV (i.e., too heavy to be transported by a small vehicle or deployed by unassisted hands; and too cumbersome to suit the tight corners of small lakes, ponds or rivers). Further, for marine safety concern, almost all the ASCs take closed form design, which makes it difficult to incorporate many existing biological sensors or water testing equipments. This restricts its applications to bathymetry survey [2] or fish-tracking [3] with a dangled side scan sonar or radio signal receiver or simply being a communication relay station for AUVs [8].

Motivated by the previous work, the work presented in the paper develops an Interactive Mobile Aqua Probe and Surveillance (IMAPS) system that crosses the lines of ROV, AUV and ASC with low cost and minimum maintenance. The robotic vehicle is designed to cruise on the surface of a given water body, take necessary data or samples with multiple sensors that can be lowered down to the water, observe and record the environment, and even search for the source of pollution. It is an ideal tool for day-to-day applications of water sampling and testing by regular schools, researchers, and environmental and biological workers.

The rest of the paper is organized as follows: the hardware and software designs are presented respectively in Section 2. The analysis of the system and its controllability is then given in Section 3. Section 4 introduces the experiments and applications we conducted so far with the apparatus. At the end, Section 5 provides the brief summary of the work and our future directions.

Manuscript received November 1, 2006; revised February 15, 2007. This work was supported by NSF under Grant DUE-0442861.

H. Zhang is with Dept. of Mechanical Engineering, Rowan University, 201 Mullica Hill Road, Glassboro, NJ 08028 (e-mail:zhang@rowan.edu); Y. Tang is with Dept. of Electrical and Computer Engineering, Rowan University (e-mail: tang@rowan.edu).

2. DESIGN OF IMAPS

For the purpose of wide adoption by the public, the development of the IMAPS adheres to the following design goals:

1) Modular design: The design should minimize the effort required to reconfigure sensors, electronics, and control systems. The entire design is partitioned into several subsystems that are easy to upgrade with users' input, which has no or little impact on others.
2) Small size and portability: The vehicle should be light enough to be handled by at most two persons and small enough to be easily put into the back of a midsized SUV or minivan. Therefore, no special equipment or vehicle will be required to use the robot.
3) Minimum maintenance: The susceptibility to corrosion and electronic faults should be minimized. The internal equipment (e.g., camera, sensors, and computer) should be protected.
4) Long operation time: The robot should be able to operate in water for at least four hours, enough for a regular morning or afternoon session. Extra battery pack can be added for longer time without affecting the performance of the robot itself.
5) Flexibility: For different tasks or applications, the robot should be able to work on different kinds of water bodies. Its operating system should also be open to accept and adapt to multiple control algorithms.
6) Easy rescue: The robot operates on water and is subject to unexpected external influences such as bad weather or curious animals. When malfunction or technical difficulty arises, it should be easy to locate and retrieve the robot.

2.1 General Structure

Following the above key characters, an agent-server approach (Figure 1) is chosen for the general structure of the IMAPS. The field agent takes the form of a model surface vehicle. Depending on working condition or design preference, it can carry different shapes, such as a torpedo, a racing boat, or a catamaran. In order to obtain the capability of maneuvering on the surface and sample the water, the agent is equipped with several interacting and cooperating units as shown in Figure 2. The units include an Actuating Module powered by solar charged batteries, an On-board Device Control Module to monitor the status of the vehicle and on-board systems, and a Winch Module to deploy the bio-sensors, such as temperature, pH, turbidity, dissolved oxygen, conductivity, chlorophyll, and ion-specific inorganic nutrients. All these modules are controlled by a mini computer, *Mini-ITX* [18], which also connects with the Bio-Data Collecting Module to retrieve data as they are collected and sends them in real time to the host station via a radio frequency (RF) transceiver. Two on-board infra-red enabled video cameras, one forward-oriented and the other downward-looking, are used to monitor the condition of the IMAPS and visually inspect field conditions in both day and night.

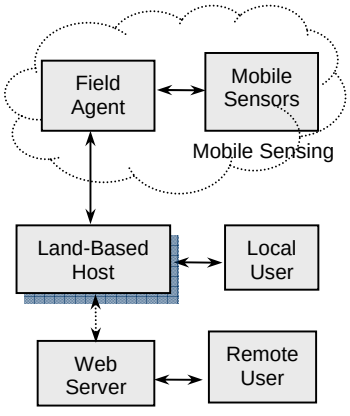

Figure 1: Block diagram of control.

As shown in Figure 3, a high end host computer is used to interactively communicate and control the agent. Real-time images and data are retrieved for analysis and display via the video receiver and RF transceiver. Users can store the data into a data log and/or display them on the screen for visual inspection. The inputs or commands from users are relayed to the agent through the RF transceiver.

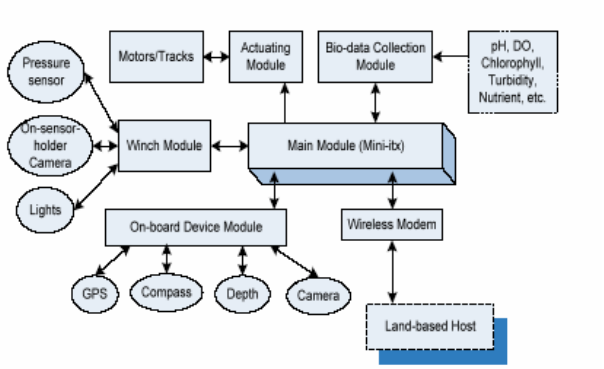

Figure 2: Block diagram of the agent.

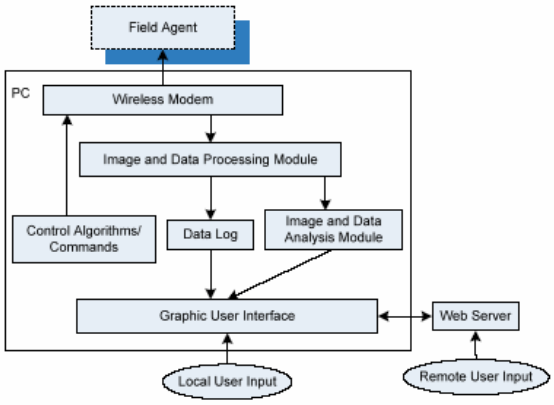

Figure 3: Block diagram of the host.

2.2 Hardware Design and Construction

Parallel to the development of the control structure, the mechanical construction has evolved from a torpedo shaped prototype as shown in Figure 4(A) to a pontoon style catamaran shown in Figure 4(B). The latter is constructed with an aluminum frame covered by plywood with fiberglass coating. The design provides sturdiness in the rough water condition. Each hull is divided into three separate water-tight cells for leaking control. The two hulls are connected by waterproof conduit for internal power and data transmission. With a moderate size (1m x 1m x 0.4m), the agent can be fit into a regular SUV or even the trunk of a full size sedan. Hence the robot can be easily transported by biological scientists and deployed at test sites that are hard to reach in traditional ways. The agent provides a fair amount of payload (about 20kg) to carry common biological or chemical sensors. The double hull design offers stability for both calm water and light waves. It also supplies a large footprint for easy placement of bio-sensors.

(a) (b)

Figure 4: The two generations of IMAPS agent system.

Inside the hulls, a battery pack with 10 Ni-MH batteries provides 12V power for up to 6 hours of running time. Up to two more battery packs can be added without changing the buoyancy and handling of the boat significantly. Extra batteries can be added for extended operating time in shallow water when a short (<10m) sensor cable can be used. The GPS, depth finder and motor controllers are all connected to the *MiniITX* computer via serial connections. Two cameras (one forward looking and one downward looking) with their video transmitters can send footages of surroundings and underwater environment to more than 1km away. A MaxStream wireless modem [17] connects the onboard computer to the host for command and data exchange up to 2km away. A foldable beam is integrated to the winch system for bio-sensor deployment. It enables the sensor to be lifted at above-water level. So the robot can test the water quality at the surface. The lift-up design also protects the sensor from hitting the bottom of the water body in shallow area and acts as an external antenna to amplify the range of wireless transmission.

2.3. Software Design

For the convenience of operating the probe for the non-engineering persons an easy-to-use graphical user interface (GUI) with two panels is developed. As depicted in Figures 5 and 6, the right panels show the GPS coordinates and depth as well as allowing users to choose either manual control or autonomous control of the field agent. Under manual control, users can use either a joystick or sliding bars to control thruster speed, while under autonomous control, where several control algorithms are deployed, users can choose several sampling stations on the map of the testing area as well as setting the depths desired for the sensors to collect data. Manual entry of desired GPS stations will be an option as well. On the left panel, users can choose to see either the video feeds from the on-board cameras of the field agent, or they can see the biological and environmental sensor data. Users are able to select the method of data display, including seeing the raw data as text, in user-defined graphs, or both formats.

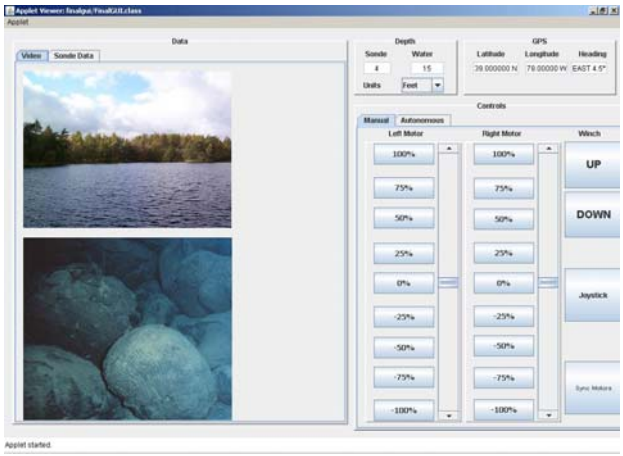

Figure 5: GUI of the IMAPS in Manual Control

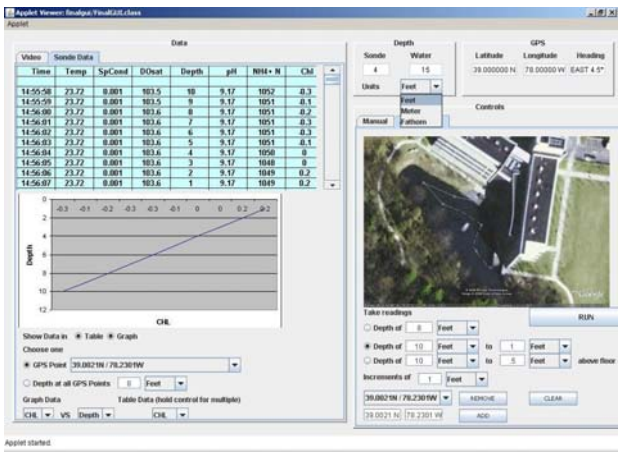

Figure 6: GUI of the IMAPS in autonomous control

3. MODELING OF THE IMAPS AGENT

The IMAPS agent is considered as a simple mechanical system acting on Lie space in our design. Without loss of

generality, let us denote the general coordinates of a robot with $q \in Q$ where the n-dimensional manifold Q is the configuration space. Then the system can be classified as a simple mechanical control system (Q; G; T; V; F) where G is a Riemannian metric that corresponds to the kinetic energy metric of the system on Q; $T = \frac{1}{2}G(\dot{q},\dot{q})$ is the kinetic energy; V is the potential energy; and F is the set of m linearly independent 1-forms on Q, which corresponds to the acting forces or torques on the system. While writing the Lagrangian of the system as $L(q,\dot{q},t) = T - V$, the dynamics of the system can be described by the forced Euler-Lagrange's equation:

$$\frac{d}{dt}\left(\frac{\partial L}{\partial \dot{q}}\right) - \frac{\partial L}{\partial q} = \sum_{i=1}^{m} u_i(t) F^i . \qquad (1)$$

where u_i is Lagrangian.

According to our design, the IMAPS agent stays on the surface of the water, which is presumably level in a limited area. Therefore, we can set the potential energy $V = 0$, and simplify the Lagrangian as

$$L(q,\dot{q}) = \frac{1}{2}G(\dot{q},\dot{q}) = \frac{1}{2}\dot{q}^T G \dot{q} . \qquad (2)$$

where $G_{ij} = \dfrac{\partial^2 L}{\partial q^i \partial q^j}$ is the metric of the system.

In mechanics, we often call $p = \frac{\partial L}{\partial q}$ the momentum [24]. Then we can rewrite the Eurler-Lagrange's equation in body coordinates as:

$$\dot{p}_a = ad_q^* p_a + \tau_a . \qquad (3)$$

where $\tau_a = g_a^e \tau_e$. It should be noted that the momentum is not constant in the body based coordinate system even if there is no external force acting on the system.

Now let us analyze acting forces on the robot. As stated earlier, the IMAPS agent takes advantage of pontoon double hull design for its intrinsic stability. The center of buoyancy of the two hulls, CB_L and CB_R, are far apart, hence provides a wide base to position the center of mass, CM, or center of Gravity, CG. For simplicity, it is assumed that the mass is evenly distributed to the left and right part of the boat, and CM is located at the centerline looking from the top. Considering the length of the boat is much greater than the height and the speed of the boat is around 1m/s, the pitch and roll angle generated by gravity, buoyancy and the thruster force is negligible. Therefore, the CM, CB_L and CB_R are vertically coplanar.

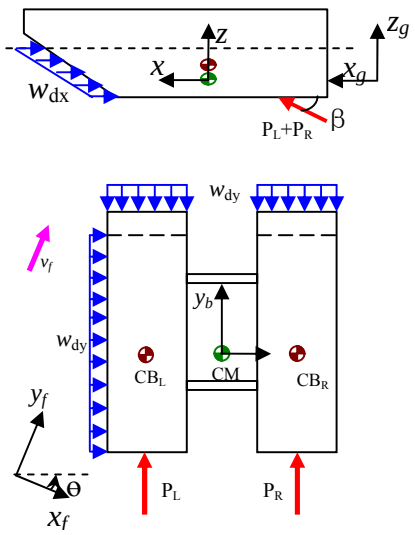

Figure 7: Force analysis of the IMAPS third design.

While the robot is operated in a calm day on a lake or a slowly moving water, the flow of the current can be considered constant. Then we set up the inertial coordinate system (also called global or fixed frame) with y direction parallel to the velocity of the flow and z direction points upward. We can then set up a body coordinate system (also called moving or body frame) with CM as the origin, y as the forward direction of the boat, x as the transverse direction, and z as the direction points upward. For simplicity, the x-y planes of the global coordinate system and body coordinate system are co-planar as shown in Figure 7. The position x and orientation θ of the vehicle can then be represented as $X = (\mathrm{x},\theta) = (x, y, z, \theta_x, \theta_y, \theta_z)$. Finally, the transformation of any vector from the body frame to the global frame can be written as

$$x_f = g_f^b X_b = \begin{bmatrix} R(\theta) & \mathrm{x} \\ 0 & 1 \end{bmatrix} X_b , \qquad (4)$$

where g_f^b is the transformation matrix from the body frame to global frame. $R(\theta)$ is the rotation matrix, x is the translation vector, and x_f and X_b are the point vector denoted in fixed and body frame respectively. Without loss of clarity, starting from this point, unless otherwise defined, we will use upper case letter to denote vectors in body frame while lower case letter to denote the same vector in global frame. Therefore, x_f and X_b can be written as x and X respectively.

The velocity vector of the vehicle, namely surge, sway, heave, roll, pitch and yaw, is written as $(\dot{\mathrm{x}},\dot{\theta}) = (\mathrm{v}^{\mathrm{T}},\omega^{\mathrm{T}}) = (v_x, v_y, v_z, \omega_x, \omega_y, \omega_z)$ or in the matrix form

$$\zeta_b = \begin{bmatrix} \Omega & \mathrm{v} \\ 0 & 1 \end{bmatrix}, \quad (5)$$

with $\Omega = \omega^{\wedge} = \begin{bmatrix} 0 & -\omega_z & \omega_y \\ \omega_z & 0 & -\omega_x \\ -\omega_y & \omega_x & 0 \end{bmatrix}$, where the lift operator ^ denotes that a vector is lifted to a skew-symmetric matrix. The lift operator provides a way to represent cross production of two vectors in a matrix form, such that

$$\omega^{\wedge} v = \begin{bmatrix} 0 & -\omega_z & \omega_y \\ \omega_z & 0 & -\omega_x \\ -\omega_y & \omega_x & 0 \end{bmatrix} \begin{bmatrix} v_x \\ v_y \\ v_z \end{bmatrix} = \omega \times v \quad (6)$$

Due to the motion of the vehicle in the fluid, the added mass and added inertia are introduced as the direct result of the acceleration of the fluid particles near the vehicle body. The accelerations of different fluid particles vary due to their distances and positions relative to the vehicle body. Then we can use added mass and inertia to denote the weighted integration of all the masses and inertia that are accelerated by the motion of the vehicle. They can be described by a 6x6 matrix in general. Since each hull of the vehicle in our design takes the symmetric and slender form, the added mass only affect the terms m_x, m_y and J_z, i.e.,

$$M = \begin{bmatrix} m & 0 & 0 \\ 0 & m+1.19l\rho a^2 & 0 \\ 0 & 0 & m+1.19l\rho a^2 \end{bmatrix} = \begin{bmatrix} m_x & 0 & 0 \\ 0 & m_y & 0 \\ 0 & 0 & m_z \end{bmatrix},$$

$$J = \begin{bmatrix} J+0.045l\rho a^4 & 0 & 0 \\ 0 & J & 0 \\ 0 & 0 & J \end{bmatrix} = \begin{bmatrix} J_x & 0 & 0 \\ 0 & J_y & 0 \\ 0 & 0 & J_z \end{bmatrix}$$

With the added mass and inertia of the vehicle, we can rewrite the Lagrangian of the system as the form of kinetic energy:

$$L = T = \tfrac{1}{2}(v^T, \omega^T) \begin{pmatrix} M & 0 \\ 0 & J \end{pmatrix} \begin{bmatrix} v \\ \omega \end{bmatrix}. \quad (7)$$

Let P and Π denote the linear and angular components of the momentum with respect to the body based coordinate system, we have

$$\begin{cases} P = \dfrac{\partial L}{\partial v} = Mv \\ \Pi = \dfrac{\partial L}{\partial \omega} = J\omega \end{cases} \quad (8)$$

Correspondingly, let p and π denote the linear and angular components of the momentum with respect to the inertial coordinate system. The relationships between those in body frame are

$$\begin{cases} p = R\mathrm{P} \\ \pi = R\Pi + \mathrm{x} \times p \end{cases}, \quad (9)$$

Without loss of clarity, we used R to denote $R(\theta)$. Noticing $R^{-1} = R^T$ for a rotation matrix, we can inverse Eq. (9):

$$\begin{cases} \mathrm{P} = R^T p \\ \Pi = R^T(\pi - \mathrm{x} \times p) \end{cases}. \quad (10)$$

Differentiate Eq. (10) and notice that $\Omega = \omega^{\wedge} = R^{-1}\dot{R}$, we have

$$\begin{cases} \dot{\mathrm{P}} = \Omega^T R^T \mathrm{P} + R^T \dot{p} \\ \dot{\Pi} = \Omega^{\mathrm{T}} R^T(\pi - \mathrm{x} \times p) + R^T(\dot{\pi} - \dot{q} \times p - q \times \dot{p}) \end{cases} \quad (11)$$

On the other hand, applying Newton's second law to the vehicle in the inertial coordinate system, we have

$$\begin{cases} \dot{p} = \sum f_i \\ \dot{\pi} = \sum \mathrm{r_i} \times f_i + \sum \tau_j \end{cases} \quad (12)$$

where $\mathrm{f_i}$ and τ_j denote external forces and torques expressed in inertial frame, $\mathrm{r_i}$ is the position vector from each force to the origin of the inertial coordinate. Substituting Eq (12) to Eq (8), and noticing that $\Omega^T(\bullet) = (\bullet) \times \omega$, we obtain

$$\begin{cases} \dot{\mathrm{P}} = \mathrm{P} \times \omega + \sum \mathrm{F_i} \\ \dot{\Pi} = \Pi \times \omega + \mathrm{P} \times \mathrm{v} + \sum \rho_i \times F_i + \sum \mathrm{T}_j \end{cases} \quad (13)$$

where terms P×ω and Π×ω+P×v are Coriolis forces, $\rho_i = \mathrm{r}_i - \mathrm{x}$ is the position vector from each external force to the origin of the body frame, $F_i = R^T f_i$ and $T_j = R^T \tau_j$ are external forces and torques denoted in body based coordinate system. In our system, the external forces are $F_L + F_R + F_{drag} + F_{wind} + F_{wave} + F_w + F_B$, where

$$F_L = \begin{bmatrix} P_L \cos\beta \\ 0 \\ P_R \sin\beta \end{bmatrix}$$

and

$$F_R = \begin{bmatrix} P_R \cos\beta \\ 0 \\ P_R \sin\beta \end{bmatrix}$$ are the left and right thruster forces of the robot, $F_{drag} = \begin{bmatrix} d_x & 0 & 0 \\ 0 & d_y & 0 \\ 0 & 0 & d_z \end{bmatrix} \begin{bmatrix} v_x \\ v_y \\ v_z \end{bmatrix}$ is the hydrodynamic drag force including friction force between the boat body and water and the wave making Froude force, F_{wave} is the wave force, F_w is the sum of wind and current force, and F_{Weitht} and F_B are weight and corresponding buoyancy forces of the boat. Note that we have

$$F_{wave} + F_w + F_{weight} + F_B = R\left(f_{wave} + f_w + f_{weight} + f_B\right)$$

With

$$f_w = \begin{bmatrix} f_w \cos\alpha_z \cos\alpha_x \\ f_w \cos\alpha_z \sin\alpha_x \\ f_w \sin\alpha_z \end{bmatrix}, \; f_{weight} = \begin{bmatrix} 0 \\ 0 \\ -mg \end{bmatrix}, \; f_B = \begin{bmatrix} 0 \\ 0 \\ V_{olum}\,\rho g \end{bmatrix}.$$

The force from wave is a complicated issue. To simplify the problem, the following assumptions are made:

1. Wave considered in the work is one dimensional plane progressive free surface wave.
2. Wave propagates along the x direction in the fixed coordinate system, and starts from the origin of the body based coordinate system.
3. Wave sizes are larger than the size of the boat, i.e., we ignore the ripples and consider them as drag.
4. Waves are not influenced by the presence of the boat.
5. Wave follows linear theory. That is, all water particles move in small circular orbits determined by the magnitude of the wave, but their mean positions do not change even the wave itself is propagating.

Follow Thompson et al. [10] with above assumptions, the equation of the wave is obtained as follows:

$$\eta(d,\tau) = A\cos(kd - w_f\tau + \varepsilon),$$

where η is the wave height at horizontal distance d from the origin of body frame, τ is time, A is the maximum wave height, k is the wave number and can be calculated from wave length λ as $k = 2\pi/\lambda$, and w_f is wave frequency. ε is the phase angle of the wave and without loss of generality, can be set as zero. Since the boat is small and does not run into very strong wave condition, most water bodies can be considered deep enough ($>\frac{1}{2}\lambda$) to satisfy the dispersal relation $\omega_f^2 = gk$. At d=0, we can obtain the slope of the wave as $\phi = -\eta(0,\tau) = -Ak\sin\omega_f\tau$, and then simplify the wave load and the gravity acceleration to one equivalent gravity acceleration as

$$g_e = g - \omega_f^2 A\cos\omega_f\tau. \tag{14}$$

Hence, we can combine the force from weight, buoyancy and wave as one single term

$$f_v = \begin{bmatrix} (V\rho - m)g_e\sin\phi \\ 0 \\ (V\rho - m)g_e\cos\phi \end{bmatrix}, \tag{15}$$

and their corresponding torque as

$$\tau_v = \begin{bmatrix} 0 \\ -V\rho g_e d_{BG} - J_y Ak\omega_f^2\sin\omega_f\tau \\ 0 \end{bmatrix}. \tag{16}$$

Therefore, we can write the governing equation of the system as Equation (17) or its expanded form Equation (18). Please note that we ignored the torque generated by drag forces and winds, since they are distributed forces acting on the entire wet and dry areas respectively.

From here, we will simplify the case of the IMAPS to a 2-D planar robot on water surface. First, assume the boat is operating on calm water and the wind is constant and parallel to the surface of the water, i.e., α_z=0. We further set the x-direction of the fixed frame as the blowing direction of wind, then we have $f_{wind} = [f_w, 0, 0]^T$ in global frame. Last, let v_z=0, $\omega_x = \omega_y = 0$ for planar case, then we have

$$\begin{cases} m_x\dot{v}_x = m_y v_y\omega_z + (P_L + P_R)\cos\beta - d_x v_x + f_w\cos\theta \\ m_y\dot{v}_y = -m_x v_x\omega_z - d_y v_y + f_w\sin\theta \\ J_z\dot{\omega}_z = (m_x - m_y)v_x v_y + (P_R - P_L)\rho_z\cos\beta - d_{rz}\omega_z \end{cases} \tag{17}$$

Rewrite it in a matrix form as Equation (19).

$$\begin{cases} \dot{\mathrm{P}} = \mathrm{P}\times\omega + \begin{bmatrix} (P_L + P_R)\cos\beta \\ 0 \\ (P_L + P_R)\sin\beta \end{bmatrix} + \begin{bmatrix} d_x v_x \\ d_y v_y \\ d_z v_z \end{bmatrix} + R\begin{bmatrix} f_w\cos\alpha_z\cos\alpha_x \\ f_w\cos\alpha_z\sin\alpha_x \\ f_w\sin\alpha_z \end{bmatrix} + R\begin{bmatrix} (V\rho - m)g_e\sin\phi \\ 0 \\ (V\rho - m)g_e\cos\phi \end{bmatrix} \\ \dot{\Pi} = \Pi\times\omega + \mathrm{P}\times\mathrm{v} + \begin{bmatrix} \rho_x \\ \rho_y \\ \rho_z \end{bmatrix}\times\begin{bmatrix} P_L\cos\beta \\ 0 \\ P_L\sin\beta \end{bmatrix} + \begin{bmatrix} \rho_x \\ -\rho_y \\ \rho_z \end{bmatrix}\times\begin{bmatrix} P_R\cos\beta \\ 0 \\ P_R\sin\beta \end{bmatrix} + R\begin{bmatrix} 0 \\ -V\rho g_e d_{BG} - J_y Ak\omega_f^2\sin\omega_f\tau \\ 0 \end{bmatrix} + \begin{bmatrix} d_{rx}\omega_x \\ d_{ry}\omega_y \\ d_{rz}\omega_z \end{bmatrix} \end{cases} \tag{17}$$

$$\begin{cases} m_x\dot{v}_x = m_y v_y\omega_z - m_z v_z\omega_y + (P_L+P_R)\cos\beta + d_x v_x + f_w\cos\alpha_z\cos\alpha_x + (V\rho - m)g_e\sin\phi \\ m_y\dot{v}_y = m_z v_z\omega_x - m_x v_x\omega_z + d_y v_y + f_w\cos\alpha_z\sin\alpha_x \\ m_z\dot{v}_z = m_x v_x\omega_y - m_y v_y\omega_x + (P_L+P_R)\sin\beta + d_z v_z + f_w\sin\alpha_z + (V\rho - m)g_e\cos\phi \\ J_x\dot{\omega}_x = (J_y - J_z)\omega_y\omega_z + (m_y - m_z)v_y v_z + (P_L - P_R)\rho_y\sin\beta - d_{rx}\omega_x \\ J_y\dot{\omega}_y = (J_z - J_x)\omega_z\omega_x + (m_z - m_x)v_z v_x + (P_L+P_R)(\rho_z\cos\beta - \rho_x\sin\beta) - V\rho g_e d_{BG} - J_y Ak\omega_f^2\sin\omega_f\tau - d_{ry}\omega_z \\ J_z\dot{\omega}_z = (J_x - J_y)\omega_x\omega_y + (m_x - m_y)v_x v_y + (P_R - P_L)\rho_z\cos\beta - d_{rz}\omega_z \end{cases} \quad (18)$$

$$\begin{bmatrix} m_x\dot{v}_x \\ m_y\dot{v}_y \\ J_z\dot{\omega}_z \end{bmatrix} = \begin{bmatrix} m_x v_x \\ m_y v_y \\ 0 \end{bmatrix} \times \begin{bmatrix} v_x \\ v_y \\ \omega_z \end{bmatrix} + \begin{bmatrix} (P_L+P_R)\cos\beta \\ 0 \\ (P_L+P_R)\rho_z\sin\beta \end{bmatrix} + \begin{bmatrix} -d_x & 0 & 0 \\ 0 & -d_y & 0 \\ 0 & 0 & -d_{rz} \end{bmatrix} \begin{bmatrix} v_x \\ v_y \\ \omega_z \end{bmatrix} + \begin{bmatrix} \cos\theta & -\sin\theta & 0 \\ \sin\theta & \cos\theta & 0 \\ 0 & 0 & 1 \end{bmatrix} \begin{bmatrix} f_w \\ 0 \\ 0 \end{bmatrix}. \quad (19)$$

Note that $\begin{bmatrix} m_x v_x \\ m_y v_y \\ 0 \end{bmatrix} = \begin{bmatrix} 1 & 0 & 0 \\ 0 & 1 & 0 \\ 0 & 0 & 0 \end{bmatrix} \begin{bmatrix} m_x & 0 & 0 \\ 0 & m_y & 0 \\ 0 & 0 & J_z \end{bmatrix} \begin{bmatrix} v_x \\ v_y \\ \omega_z \end{bmatrix}$

and

define $I_0 = \begin{bmatrix} 1 & 0 & 0 \\ 0 & 1 & 0 \\ 0 & 0 & 0 \end{bmatrix}$, $M = \begin{bmatrix} m_x & 0 & 0 \\ 0 & m_y & 0 \\ 0 & 0 & J_z \end{bmatrix}$, $V = \begin{bmatrix} v_x \\ v_y \\ \omega_z \end{bmatrix}$,

$D = \begin{bmatrix} -d_x & 0 & 0 \\ 0 & -d_y & 0 \\ 0 & 0 & -d_{rz} \end{bmatrix}$, then we have

$$M\dot{V} = (I_0 MV)\hat{}\, V + DV + Rf_w + U. \quad (20)$$

Let $V = \dot{X}$. Then we get

$$M\ddot{X} = (I_0 M\dot{X})\hat{}\,\dot{X} + D\dot{X} + Rf_w + U. \quad (21)$$

If we choose $U = -(I_0 M\dot{X})\hat{}\,\dot{X} - D\dot{X} + PID$, then we can enforce PID control to the IMAPS agent to achieve desired result. For example, if we define the error function

$$e = E(X - X_0). \quad (22)$$

where $E \in R^{3\times3}$ is a full rank matrix, and X_0 is the desired trajectory of the agent. We choose input as

$$U = -(I_0 M\dot{X})\hat{}\,\dot{X} - D\dot{X} + \lambda e + M^{-1}\ddot{X}_0. \quad (23)$$

Then we have

$$\ddot{X} = M^{-1}Rf_w + M^{-1}\lambda e + \ddot{X}_0. \quad (24)$$

Note that

$$\begin{aligned} \ddot{e} &= E(\ddot{X} - \ddot{X}_0) \\ &= E(M^{-1}Rf_w + M^{-1}\lambda e + \ddot{X}_0 - \ddot{X}_0) \\ &= EM^{-1}(Rf_w + \lambda e) \end{aligned} \quad (25)$$

Then if we choose $E=M$, then the error dynamics follows as

$$\ddot{e} = Rf_w + \lambda e. \quad (26)$$

By choosing Lyapunov function as $V = 1/2\left(e^2 + \dot{e}^2\right)$, it is easy to show that the tracking is asymptotically stable for $\lambda<-1$ under the condition that the wind and current force is sufficiently weak.

4. EXPERIMENTS AND PERFORMANCE

Intensive experiments have been conducted on the IMAPS. Figure 6(a) shows the IMAPS running on Little Egg Bay of New Jersey, a local sea shore. In a mildly windy day with about 20~40 km/h wind speed and 0.05~0.1m wave height, the robot can obtain up to 1m/s speed when venturing against the wind toward the open sea.

(a)

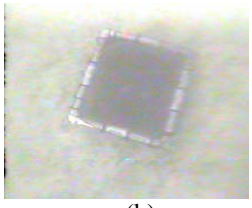

(b)

Figure 6: (a) The second generation IMAPS is under test in Little Egg Bay, NJ. (b) Photo of a researching apparatus taken by the second generation Video Probe.

Figure 6(b) is a photo taken by the IMAPS in field when studying the ecology of an endangered species of sea grass [17] at the Jupiter Inlet of Florida. The task is to analyze the influence of human activities, such as boating and seashore constructions, on the growth and survival of sea grass that is typical to the area. The traditional way of doing this research needs to physically snorkel or scuba 1 to 3 meters deep into the area where sea grass grows and manually count the leaf numbers per square foot. With the help of the IMAPS, several snapshots of the sea grass can be easily obtained and fed to image processing software for the analysis of its color as well as the density distribution.

A comparative field test was also performed to evaluate the efficiency of the robot, where water temperature, pH, and dissolved oxygen data of Rowan pond were collected at

10 waypoints using both the IMAPS and the manual operations. In the manual operation, two persons used a handheld GPS receiver to locate the waypoints, and then anchored the canoe. While one was controlling the depth of a YSI™ Sonde, a multipurpose biological sensor, under the water, the other recorded the data manually. The entire data collection process was conducted over a two-day period with over 7 hours on water. In comparison, the same experiment took less than 20 minutes with only one operator remotely controlling the IMAPS. Using the collected data points, several 3D contour plots were created using GIS software, as the one shown in Figure 7 of the surface temperature and depth distributions on Rowan Pond.

Although the full intelligent control of the robot is still under development, some initial tests were performed for simple point tracking. In Figure 8, the robot was directed to travel from GPS point A(75.08547, 39.43875) and facing west to point B(75.08540, 39.43910) on the water surface of a local lake. Using the drag coefficient $d_x=d_y=d_{rz}=0.1$, $m_x=m_y=16$kg, $J_z=1.2$kg·m^2, and simply choosing a proportional controller after factoring the velocity calculated from GPS data, the robot can autonomously travel from point A to point B. In the figure, the trajectory of the robot is plotted against the surface of the lake, which is shown as the dark area. The robot steered itself, resisted the wind and light current, and reached and stayed at the desired point.

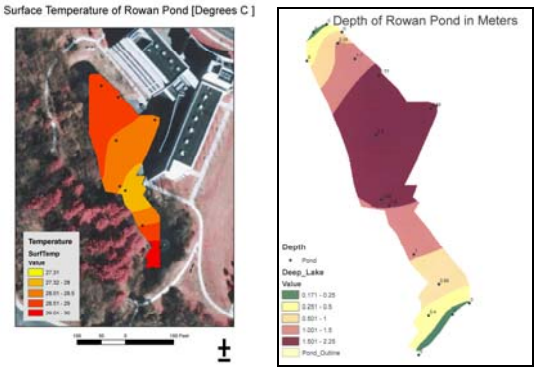

Figure 7: Surface temperature plot (left) and Bathymetry plot (right) of Rowan Pond.

Figure 8: Experimental result of IMAPS on a local lake.

5. CONCLUSION AND FUTURE WORK

The IMAPS has successfully achieved its major development goals, providing researchers and educators a low-cost and expandable platform for ecological and biological study. A series of experimental tests have proved that the IMAPS is flexible and efficient in real-time remote data acquisition of aquatic habitats.

Future development on the support infrastructure for the IMAPS can be extended in several directions. For instance, while keeping the core hardware control behind the user interface, more advanced high-level control algorithms can be designed based on users' needs and integrated into the field-deployable unit. Such algorithms that are under development include autonomous sampling data with the given testing points by a user, and automatically seeking out the source of a pollutant by measuring the pollutant and identifying a concentration gradient, and navigating up-gradient. Considering other complex terrains, such as marsh and creek, another interesting development would be upgrading the IMAPS with amphibious capability to travel on both water and land.

Acknowledgment: This material is based upon work supported by the National Science Foundation under Grant No. 0442861.

Reference:

1. A. Pascoal, P. Oliveira, C. Silvestre, L. Sebastiao, M. Rufino, V. Barroso, J. Gomes, G. Ayela, P. Coince, M. Cardew, A. Ryan, H. Braithwaite, N. Cardew, J. Trepte, N. Seube, J. Champeau, P. Dhaussy, V. Sauce, R. Moitie, R. Santos, F. Cardigos, M. Brussieux, and P. Dando, Robotic ocean vehicles for marine science applications: the European ASIMOV Project, *OCEANS 2000 MTS/IEEE Conference and Exhibition*, Vol. 1, pp. 409 -- 415, 2000.

2. B.S. Bourgeois, A.B. Martinez, P.J. Alleman, J.J. Cheramie, J.M. Gravley, Autonomous Bathymetry Survey System, *IEEE Journal of Oceanic Engineering*, Vol. 24, No. 4, pp: 414-423, Oct. 1999.

3. C.A. Goudey, T. Consi, J. Manley, M. Graham, B. Donovan, L. Kiley, A Robotic Boat for Autonomous Fish Tracking, *Marine Technology Society Journal*, Vol. 32, No. 1, pp. 47-53, 1998.

4. B. Horling, R. Vincent, R. Mailler, J. Shen, R. Becker, K. Rawlins, and V. Lesser, Distributed Sensor Network for Real Time Tracking, *In Proceedings of the 5th International Conference on Autonomous Agent*, June, 2001.

5. L. Matthies, Erann Gat, Reid Harrison, Brian Wilcox, Richard Volpe, Todd Litwin, Mars Microrover Navigation: Performance Evaluation and Enhancement. Autonomous Robots, *Special Issue on Autonomous Vehicles for Planetary Exploration*, Vol. 2, No. 4, pp. 291--311, 1995.

6. J. A. Farrell, Shuo Pang, and Wei Li, Chemical Plume Tracing via an Autonomous Underwater Vehicle, *IEEE Journal Of Oceanic Engineering*, Vol. 30, No. 2, pp428-442, April 2005.

7. J. Curcio, J. Leonard, and A. Patrikalakis. SCOUT --- A Low Cost Autonomous Surface Platform for Research in Cooperative Autonomy, In *Proceedings of MTS/ IEEE OCEANS Conference and Exhibition 2005*, Washington DC, pp. 730-735, Sept., 2005.
8. J. Curcio, J. Leonard, J. Vaganay, A. Patrikalakis, A. Bahr, D. Battle, H. Schmidt, and M. Grund, Experiments In Moving Baseline Navigation Using Autonomous Surface Craft, In *Proceedings of MTS/ IEEE OCEANS Conference and Exhibition 2005*, Washington DC, pp. 290-294, Sept. 2005.
9. J. E. Manley, A. Marsh, W. Cornforth, and C. Wiseman, Evolution of the Autonomous Surface Craft AutoCat**.** *In Proceedings of MTS/IEEE OCEANS Conference and Exhibition 2000*, Vol. 1, pp.403--408, 2000
10. J.M.T. Thompson, R.C.T. Rainey and M.S. Soliman, Mechanics of Ship Capsize under Direct and Parametric Wave Excitation, *Philosophical Transactions: Physical Sciences and Egnineering, Nonlinear Dynamics of Engineering System,* Vol. 338, No. 1651, pp.471-490, 1992.
11. J. P. Dunne, A. H. Devol, and S. Emerson, The oceanic remote chemical/optical analyzer (ORCA) – an Autonomous Moored Profiler, *Journal of Atmospheric and Oceanic Technology*: Vol. 19, No. 10, pp. 1709–1721, 2002
12. J. Porter, P. Arzberger, H. Braun, P. Bryant, S. Gage, T. Hansen, P. Hanson, C. Lin, F. Lin, T. Kratz, W. Michener, S. Shapiro, and T. Williams, Wireless Sensor Networks For Ecology, *BioScience*, Vol. 55, No. 7, pp561-572, July 2005.
13. M. Dunabin, J. Roberts, K. Usher, and P. Corke. 2004. A New Robot for Environmental Monitoring On the Great Barrier Reef. *In Proceedings of 2004 Australasian Conference on Robotics and Automation*. Canberra, Australia, Dec. 2004.
14. M. Fujita, M. Veloso, W. Uther, M. Asada, H. Kitano, V. Hugel, P. Bonnin, J. Bouramoué, and P. Blazevic. Vision, Strategy, and Localization Using the Sony Legged Robots at RoboCup-98. *AI Magazine*, 21(1):47–56, Spring 2000.
15. M. Neal, A Hardware Proof of Concept of a Sailing Robot for Ocean Observation, *IEEE Journal of Ocean Engineering*, Vol. 31, No. 2, pp. 462-- 469, April, 2006.
16. Macroinvertebrate Field and Laboratory Methods for Evaluating the Biological Integrity of Surface Waters (EPA 600-4-90-030).
17. MaxStream Website, http://www.maxstream.net/products/
18. Mini-ITX website, http://www.mini-itx.com/
19. N. J. Eiseman, ,and C. McMillan. A New Species of Seagrass, Halophilia Johnsonii, from the Atlantic Coast of Florida. *Aquatic Botany*, Vol. 9, pp. 15-19, 1980.
20. P. T. Wolter, C. A. Johnston and G. J. Niemi, Mapping Submergent Aquatic Vegetation In The US Great Lakes Using Quickbird Satellite Data, *International Journal of Remote Sensing*, Vol. 26, No. 23/10, pp.5255 – 5274, Dec. 2005.
21. R. D. Ballard, The MEDEA/JASON Remotely Operated Vehicle System. *Deep Sea Research,* Vol. 40, pp.1673-1687, 1993.
22. T. A. Henzinger and P. Ho, HyTech: The Cornell HYbrid TECHnology Tool, *Hybrid Systems*, Lecture Notes in Computer Science 999, Springer-Verlag, pp 265-294, 1995.
23. T. C. Dawe, D. S. Stakes, P. R. McGill, J. Barry, and S. Etchemendy. 1998. Subsea Instrument Deployments: Methodology And Techniques Using A Work Class Remotely Operated Vehicle (ROV). *In Proceedings of MTS/IEEE OCEANS Conference and Exhibition*, pp. 1589-1593, Nice, France, 1998.
24. V.I. Arnold, Mathematical Methods of Classical Mechanics, 2nd Edition, Springer-Verlag, New York, Inc., 1989

Dr. Hong Zhang received his bachelor's degree from the Department of Automotive Engineering of Tsinghua University, Beijing, China at 1994. He then obtained his master's and doctor's degree from the Department of Mechanical Engineering and Applied Mechanics of University of Pennsylvania, Philadelphia, at 1997 and 2000 respectively. Dr. Zhang is now an assistant professor at the Department of Mechanical Engineering of Rowan University. His research interest includes robotics, visual servo control, underactuated systems, and mechatronic design.

Dr. Ying Tang (S'99- M'02) received the B.S. and M.S. degrees from the Northeastern University, P. R. China, in 1996 and 1998, respectively, and Ph. D degree from New Jersey Institute of Technology, Newark, NJ, in 2001.

Dr. Tang is currently an Assistant Professor of Electrical and Computer Engineering at Rowan University, Glassboro, NJ. Her research interests include modeling and scheduling of computer-integrated systems, Petri nets and applications, Artificial Intelligence, Reconfigurable systems design, Networking and communication, and System-on-Chip design. She is a member of the IEEE Systems, Man and Cybernetics and Sigma Xi.